LIMNOLOGY and OCEANOGRAPHY

ASLO

Limnol. Oceanogr. 71, 2026, e70357

doi: 10.1002/lno.70357

RESEARCH ARTICLE

Long-lived subsurface anticyclonic eddy enhances microbial diversity and vertical niche partitioning

Ying Wang,[1,2] Zhaomin Han,[1,2] Lei Wang,[3] Peng Cheng,[4] Dapeng Xu,[4] Bangqin Huang,[1,2,4*] Ping Sun[1,2*]

[1]Fujian Province Key Laboratory for Coastal Ecology and Environmental Studies, Xiamen University, Xiamen, China; [2]National Observation and Research Station for the Taiwan Strait Marine Ecosystem, Xiamen University, Zhangzhou, China; [3]Third Institute of Oceanography, Ministry of Natural Resources, Xiamen, China; [4]State Key Laboratory of Marine Environmental Science, College of Ocean and Earth Sciences, Institute of Marine Microbes and Ecospheres, Xiamen University, Xiamen, China

Abstract

Subsurface anticyclonic eddies (SAEs) reshape ocean stratification and nutrient–light regimes, yet their microbial and biogeochemical impacts remain poorly resolved. We combined CTD-ADCP hydrography, nutrient profiles, microscopy and flow-cytometry, and 18S/16S rRNA transcript sequencing to examine a long-lived SAE in the northern South China Sea. The lens-shaped eddy featured a strong velocity core (maximum 0.46 m s^{-1} at 90 m) and a deepened euphotic zone from exterior reference to edge to center (107.9 → 117.9 → 124.5 m). Depth-integrated chlorophyll-*a* (25–150 m) was higher inside the eddy (19.7 mg m^{-2}) than at reference waters (18.2 mg m^{-2}), peaking at the center (20.8 mg m^{-2}), indicating subsurface intensification of autotrophic biomass. Alpha-diversity enhanced within the eddy, especially at its edge, while vertical turnover of protistan and bacterial assemblages exceeded center–edge differences, contrasting with surface-intensifying anticyclonic eddies that often homogenize communities. Distance-based redundancy analyses identified water mass, nutrient, viral, bacterial, and nanoflagellate gradients as key correlates of community structure, reflecting light-nutrient colimitation modulated by top-down control. Ecotype-resolved patterns supported this framework that high-light *Ostreococcus tauri* declined, whereas low-light *Prochlorococcus* MIT9313 was ~ 5-fold enriched just above the core and toward the center. Protist–bacteria co-occurrence network formed depth- and edge-specific modules and hub taxa included protist Stramenopiles, free-living Alphaproteobacteria and particle-associated Deltaproteobacteria. Collectively, the deepened euphotic zone and elevated subsurface chlorophyll-*a*, together with spatially structured community assembly, demonstrate that the eddy functions as a localized biogeochemical reactor enhancing subsurface productivity and microbial recycling in oligotrophic waters—linking eddy physics to ecosystem function.

Mesoscale eddies, typically spanning 100–200 km in diameter, account for over half of oceanic kinetic energy and redistribute heat, salt, and nutrients on regional to basin scales (Carton 2001; Chelton et al. 2011). By uplifting or depressing isopycnals, cyclonic and anticyclonic eddies modulate nutrient fluxes into the euphotic zone, triggering phytoplankton blooms and altering mixed-layer depth, with cascading impacts on bacteria and protists (McGillicuddy et al. 1999; Nelson et al. 2014). Although these physical–biogeochemical couplings are well documented, the responses of entire microbial assemblages, especially at trophic and ecotypic resolution, remain poorly explored.

Recent work has revealed that eddy polarity and developmental stage exert strong control over protistan metabolic activity and community composition (Beatty et al. 2025). In particular, Anticyclonic eddies, with their nutrient-poor waters, select for mixotrophic dinoflagellates and chrysophytes, upregulating genes for both phototrophy and grazing (Gleich et al. 2024). Eddy-mediated shifts in diatom size

*Correspondence: bqhuang@xmu.edu.cn; psun@xmu.edu.cn

Associate editor: Hans-Peter Grossart

Ying Wang and Zhaomin Han contributed equally to this study.

structure further cascade through the microbial food web (Waga et al. 2019). However, most investigations have focused on single phytoplankton taxa, overlooking heterotrophic and parasitic protists as well as the dichotomy between free-living and particle-associated bacteria (Nelson et al. 2014; Wang et al. 2018). In oligotrophic gyres, gradients of light, temperature and nutrients structure the distribution of *Prochlorococcus* high-light and low-light ecotypes (Moore and Chisholm 1999; Malmstrom et al. 2010) and partition picoeukaryote lineages such as *Ostreococcus* across frontal zones (Demir-Hilton et al. 2011; Clayton et al. 2017; Simmons et al. 2016). Importantly, Sheyn et al. (2025) demonstrated that cyclonic eddies enrich high-light I *Prochlorococcus* near the deep chlorophyll maximum, an effect absent in anticyclonic counterparts, underscoring eddy polarity as a determinant of microbial ecotype-level structure.

Subsurface anticyclonic eddies (SAEs) represent a unique class of coherent vortices, characterized by lens-shaped cores bounded by the main and seasonal thermoclines. Also known as intrathermocline eddies, submesoscale coherent vortices, or mode-water eddies, these structures are marked by a depressed main thermocline, uplifted seasonal thermocline, a subsurface velocity maximum, weakened stratification, and low potential vorticity (Dugan et al. 1982; McWilliams 1985; McGillicuddy et al. 1999). These attributes enable them to isolate and transport water masses across long distances, often without leaving strong surface signatures (Meunier et al. 2018; Yang et al. 2019). Their detection typically requires in situ instrumentation such as ADCP, Argo floats, gliders, or moorings (Takikawa et al. 2005; Nan et al. 2017). Despite their frequency and potential ecological importance, the influence of SAEs on protistan, free-living and particle-associated bacterial assemblages has been poorly addressed.

The South China Sea (SCS) is one of the most eddy-active regions globally, averaging 33 mesoscale eddies annually between 1993 and 2007 (Sun et al. 2021). Nearly half of the winter Kuroshio Loop Current (KLC) shedding eddies persist into late spring as subsurface, lens-shaped anticyclonic eddies (Xu et al. 2023). Unlike surface-intensified eddies, the long-lived SAEs that develop in this region have not been systematically studied in terms of their effects on microbial communities. In late 2020, one such SAE formed and remained active until late 2021 (Qi et al. 2022). It exhibited hallmark features of SAE structure—a lens structure between 25 and 150 m, a subsurface velocity maximum exceeding 0.5 m s^{-1} at $\sim$ 90 m. Unlike regular subsurface eddies, this SAE showed significant surface signals such as positive sea-level anomalies and negative sea surface temperature anomalies, reflecting KLC shedding, winter cooling, and geostrophic adjustment (Qi et al. 2022; Xu et al. 2023). Even at 11 months of age, this eddy maintained a shallower mixed layer and colder, saltier upper waters (25–50 m) than the surrounding region (Fig. 1).

Despite the prevalence of long-lived SAE in the South China Sea, it remains unclear (i) how their lens-shaped hydrography partitions microbial diversity along vertical (above-core, core, below-core) and horizontal (center–edge) gradients, (ii) whether apparent center–edge contrasts persist after accounting for vertical stratification, and (iii) how within-eddy light and nutrient regimes select for distinct trophic strategies and phototroph ecotypes. To address these questions, we coupled hydrographic observations (sea-level anomaly, ADCP, CTD) with nutrient profiles, microscopy and flow-cytometric cell counts, and 18S/16S rRNA transcript sequencing to characterize active protist, free-living bacterial, and particle-associated bacterial communities at four depths (surface, 75, 100, and 150 m) across the eddy center, edge, and adjacent reference stations. Specifically, we asked whether (1) the SAE generates distinct vertical and horizontal microhabitats that differentially structure protist, free-living, and particle-associated bacterial communities; (2) light-nutrient gradients favor mixotrophic protists in the nutrient-poor center and autotrophic protists at the nutrient-enriched edge; (3) phototrophic ecotypes partition the eddy lens according to light adaptation (e.g., low-light *Prochlorococcus* enriched within the core, high-light *Ostreococcus* above and at the edge); (4) microbial co-occurrence networks delineate modules corresponding to these hydrographic habitats. Together, these analyses aim to elucidate how SAEs reorganize microbial diversity, trophic strategies, and protist–bactria interactions, thereby linking mesoscale physical dynamics to microbial and biogeochemical functioning in one of the ocean's most eddy-active regions.

Materials and methods

Cruise logistics and study area

Data were collected aboard R/V Dong Fang Hong 3 during the NORC2021-05 cruise (20 August–8 September 2021), which targeted mesoscale eddies in the northeastern South China Sea (Nan et al. 2011). The three-dimensional structure, formation mechanism, and regional prevalence of the focal subsurface anticyclonic eddy have been described in Qi et al. (2022) and Xu et al. (2023). Building on that physical framework, we here detail the biological sampling and associated measurements. The eddy's position was tracked with a spatial resolution of 0.25° × 0.25°, using satellite altimeter-based sea-level anomalies data sourced from the Copernicus Marine Environment Monitoring Services. Stations with sea-level anomalies > 30 cm were designated eddy center, while those with sea-level anomalies < 30 cm defined eddy edge. Two hydrographic sections across the subsurface anticyclonic eddy were conducted to characterize its structure. Eleven profiles were located within the eddy, and three additional profiles served as exterior reference sites outside its influence (Fig. 1; Supporting Information Table S1).

Hydrographic data were obtained using a Sea-Bird CTD profiler (SBE 911, Sea-Bird Electronics, USA) mounted on a General Oceanics rosette sampler equipped with 24 Niskin bottles

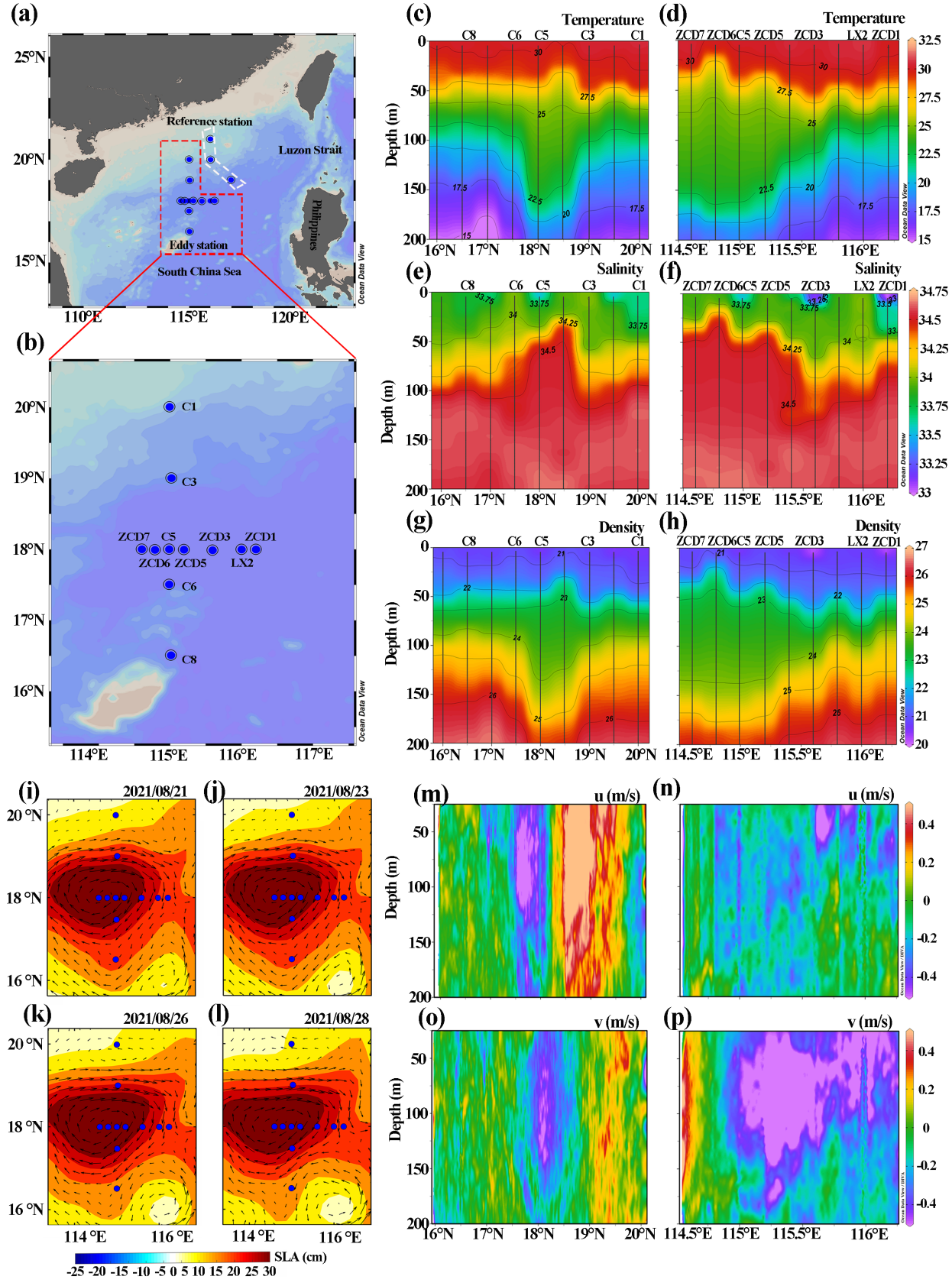

Fig. 1. Legend on next page.

(12 L capacity). The CTD's temperature and salinity data were validated by the National Center of Ocean Standards and Metrology and processed using SBE Processing Data software (v7.26.7) following the "Specifications for Oceanographic Survey." A shipborne broadband Acoustic Doppler Current Profiler (ADCP; 75 kHz; Teledyne RD Instruments, Poway, CA, USA) provided velocity profiles of the water column up to 200 m depth, with a bin size of 8 m and a sampling interval of 1 min. Velocity data were used to quantify the eddy's dynamic features, particularly its core at ~ 90 m depth. Maps of sampling transects and velocity fields were created using Matlab (R2021b, MathWorks Inc., USA). Water samples were collected from four depths (5, 75, 100, and 150 m) at each station. The 5 m samples were excluded from subsequent microbial and environmental analyses because the subsurface anticyclonic eddy was confined to 25–150 m. Analyses therefore focused on samples representing the eddy's interior across this depth range. The euphotic depth (Z_{eu}) was estimated following the inherent optical property–based model of Lee et al. (2007) and Wu et al. (2021), extracting from the 8 d–composite and 4 km–resolution level–3 data files (reprocessing R2022.0.1) generated by using NASA Earthdata's SeaDAS software. Z_{eu} was defined as the 0.5% photosynthetically available radiation (PAR) depth ($Z_{0.5\%}$), which more accurately represents the compensation depth than the conventional $Z_{1\%}$. Calculated Z_{eu} values were 107.9 m at the reference station, 117.9 m at the eddy edge, and 124.5 m at the eddy center, indicating a progressively deepened euphotic layer toward the anticyclonic center.

Biochemical observations

Water samples for chlorophyll-*a* analysis (500–1000 mL) were filtered through GF/F glass fiber filters (Whatman, UK) under low vacuum pressure (< 100 mmHg), flash-frozen in liquid nitrogen, and stored at −80°C. In the laboratory, chlorophyll-*a* was extracted in 90% acetone (16–24 h, dark, −20°C) and quantified with a Trilogy fluorometer (Turner Designs, USA) following standard fluorometric methods (Parsons et al. 1984). Depth-integrated chlorophyll-*a* (25–150 m) was calculated for each station using chlorophyll-*a* concentrations measured at standard depths (25, 50, 75, ~ 90, 100, ~ 120, and 150 m). Integrations were performed using the trapezoidal method to approximate the vertical distribution of chlorophyll-*a* within the eddy. Nutrient concentrations (nitrite, nitrate, phosphate, and silicate) were determined using an AA3 nutrient autoanalyzer (SEAL Analytical, Germany) with detection limits of 0.01–0.02 μmol L^{-1} (Du et al. 2013). Nanoflagellate abundances were quantified from 50 mL seawater samples prefiltered through a 20 μm nylon mesh. Samples were fixed with 1% glutaraldehyde and stained with DAPI (Sigma, USA) to distinguish pigmented nanoflagellates from heterotrophic nanoflagellates under fluorescence microscopy (Nikon ECLIPSE 90i, Japan). Bacterial and viral abundances were determined via flow cytometry (Epics Altra II, Beckman Coulter, USA) after fixation with 1% glutaraldehyde, flash-freezing, and staining with SYBR Green I (1/10,000 or 1/20,000 final concentration for bacteria and viruses, respectively). Viral samples were further heated to 80°C for 10 min before analysis.

RNA sampling, extraction, PCR, and sequencing

Eight liters of seawater were sequentially filtered through 200, 3, and 0.22 μm pore-size polycarbonate filters (Millipore, USA) to separate free-living and particle-associated bacteria, as well as protists. The 0.22–3 μm fraction was used for free-living bacteria, while the > 3 μm fraction represented particle-associated bacteria. Protistan communities were collected using a combination of the 0.22 and 3 μm filters to capture both small flagellates and larger microeukaryotes. For each station and depth, total RNA was extracted separately from the 3 and 0.22 μm filters, and the resulting RNA extracts were then combined by pooling equal volumes from each filter prior to DNase treatment, reverse transcription, and PCR amplification. Filters were flash-frozen in liquid nitrogen and stored at −80°C. Given environmental DNA's persistence in marine environments (Dell'Anno and Corinaldesi 2004) and the prevalence of dormant cells among marine microbes (Zinger et al. 2012), we employed a rRNA gene transcript-based approach to specifically characterize the active microbial response to eddy. RNA extraction was performed using the RNeasy Mini Kit (Qiagen, Germany), with DNA removed by RNase-free DNase treatment. cDNA was synthesized using a High-Capacity cDNA Reverse Transcription Kit (Applied Biosystems, USA). We note that rRNA read proportions do not represent absolute cell counts or biomass, but rather the distribution of ribosome-rich, metabolically active taxa under the sampled conditions (*see* Discussion for implications). For bacterial communities, the V3–V4 region of the 16S rRNA gene was amplified using primers 341F and 806R (Roggenbuck et al. 2014). The 806R primer can underestimate the relative abundance of SAR11 (Apprill et al. 2015). Therefore, our SAR11 estimates should be considered conservative. We focus on relative patterns across habitats and depths rather than absolute contributions for this clade. The comparatively low SAR11 signal may also reflect the transcript-based sequencing approach, which emphasizes ribosome-rich, metabolically

Fig. 1. Overview of hydrographic conditions in the South China Sea during the field sampling. (**a**) Map showing the broader geographic view of the sampling region. (**b**) Enlarged view of the specific sampling locations. (**c**, **d**) Temperature distributions along latitudinal and longitudinal transects, respectively. (**e**, **f**) Salinity distributions along the same transects. (**g**, **h**) Potential density distributions along latitudinal and longitudinal transects. (**i**–**l**) Sea level anomaly (cm) patterns during the sampling period, with arrows representing sea surface currents. (**m**, **n**) Zonal (u) and (**o**, **p**) meridional (v) velocity components along latitudinal and longitudinal transects.

active taxa. For protistan communities, the V4 region of the 18S rRNA gene was amplified using primers TAReuk454FWD1 and TAReukREV3 (Stoeck et al. 2010). Amplicons were pooled, purified, and sequenced using the Illumina MiSeq PE300 platform (Majorbio Bioinformatics Technology Co., Ltd., China).

Sequencing data processing and statistical analyses

Raw reads were processed using USEARCH v10 (Edgar 2013) and QIIME v1.9.0 (Caporaso et al. 2010). Quality control included trimming low-quality reads (Trimmomatic v0.38) and removing chimeras and singletons (USEARCH v10). Operational taxonomic units were clustered at 97% identity and annotated against the Protist Ribosomal Reference Database (PR2) and SILVA v132 (Guillou et al. 2013; Quast et al. 2013). Rarefied operational taxonomic unit tables ensured uniform sequencing depth for downstream analysis, with 30,036 and 20,305 reads retained for protistan and bacterial communities, respectively. Alpha diversity indices, including operational taxonomic unit richness, Chao1, ACE, and Faith's PD, were calculated using QIIME v1.8.0. Nonparametric statistical tests (Wilcoxon rank-sum and Kruskal–Wallis) were applied to evaluate diversity differences across depth layers and horizontal zones. Principal Coordinates Analysis (PCoA) and Analysis of Similarity (ANOSIM) were used to assess beta diversity using Bray–Curtis distance matrices. Differential operational taxonomic units between depth layers and between center-edge were identified using a two-step procedure. Prior to differential analysis, rare operational taxonomic units were removed, defined as those with a relative abundance < 0.01% within the eddy dataset, and the remaining operational taxonomic units were considered non-rare. Indicator Species Analysis (Indicspecies) first detected operational taxonomic units characteristic of specific spatial groups, and these were then validated using likelihood ratio tests in *edgeR*. Only operational taxonomic units identified as significant by both methods (FDR-adjusted $p < 0.05$) were designated as reliable indicators. To relate community patterns to environmental gradients, Mantel tests and distance-based redundancy analysis (dbRDA) were performed. Bray–Curtis dissimilarities of log-transformed operational taxonomic unit tables were used as response matrices, while Euclidean distances of standardized environmental variables, including temperature, salinity, dissolved inorganic nutrients, chlorophyll-*a*, viral abundance, bacterial abundance, and heterotrophic nanoflagellate abundance, served as predictors. Mantel correlations (Spearman's *r*, 9999 permutations) identified significant associations between community composition and environmental gradients. dbRDA (vegan v2.6-4, R v3.6.1) quantified the relative contributions of physicochemical and biological factors to β-diversity, with significance assessed by permutation ($p < 0.05$). To minimize collinearity, nutrient; bacterial and viral; heterotrophic and pigmented nanoflagellate; and temperature–salinity variables were summarized as principal components ($PC1_{nutrient}$, $PC1_{bac\&vir}$, $PC1_{NF}$, and $PC1_{TS}$, respectively). Mantel tests were also applied to the subset of differential operational taxonomic units to examine how vertical and horizontal enrichments (e.g., Dinophyceae, Bacillariophyta) corresponded with environmental and biological gradients within the eddy. A co-occurrence network was constructed to explore the relationships between protists and bacteria. To minimize noise and complexity in the network analysis, operational taxonomic units with a relative abundance below 0.01% and present in less than 50% of the samples were excluded. Spearman's rank correlation coefficients (*r*) were calculated for the remaining operational taxonomic units using the Hmisc package. Only robust correlations ($|r| \geq 0.7$) that were statistically significant (FDR-adjusted $p < 0.01$) were included in the analysis. Network visualization and modular analysis were carried out using the interactive software Gephi (version 0.9.2; Bastian et al. 2009).

Results

Physical, chemical, biological features

Sampling stations were arranged along two transects—C (latitudinal) and ZCD (longitudinal)—with sea-level anomalies > 30 cm stations (C5, C6, ZCD7, ZCD6, ZCD5) designated as eddy center, and sea-level anomalies < 30 cm stations (C1, C8, C3, ZCD1, ZCD3, LX2) as eddy edge (Fig. 1; Supporting Information Table S1). The eddy's vertical core was defined by maximum currents (~ 0.46 m s^{-1}) at ~ 90 m, with sharply reduced velocities above and below this depth (Fig. 1m–p). To disentangle vertical and horizontal patterns within the subsurface anticyclonic eddy, we adopted a hierarchical analytical framework. First, to characterize vertical structuring, samples were grouped into three layers relative to the velocity core (~ 90 m): above-vertical core (AVC, 75 m), vertical core (VC, 100 m), and below-vertical core (BVC, 150 m). These depth layers included all within-eddy stations (center and edge) to capture the overall vertical organization of microbial assemblages. Second, to assess horizontal structuring, all depths were combined to compare communities between the eddy center and edge. To further evaluate location-specific vertical stratification, vertical variation was analyzed separately for center, edge, and reference stations. Finally, horizontal variation within each depth layer (center vs. edge at 75, 100, and 150 m) was also tested. This nested design enabled parallel evaluation of vertical and horizontal community differentiation within and across eddy habitats.

The subsurface anticyclonic eddy (SAE) sampled in the northern South China Sea was characterized by a lens-shaped core spanning ~ 25–150 m, bounded by highly stretched isotherms and isopycnals (Fig. 1). Unlike regular subsurface eddies, this SAE exhibited significant surface signals (sea-level anomalies + 39.85 cm; cold-core sea surface temperature anomaly 0.4–1.0°C) (Fig. 1). The temperature difference between the layer above the vertical core (75 m) and below it (150 m) was 4.4°C, compared to 5.7°C at adjacent reference stations, reflecting the stretched isotherms of this eddy. A deepened

euphotic zone was observed from reference to edge to center (107.9 → 117.9 → 124.5 m), consistent with the anticyclonic downwelling signature. Depth-integrated chlorophyll-*a* (25–150 m) was higher inside the eddy (19.7 mg m^{-2}) than at reference waters (18.2 mg m^{-2}), peaking at the center (20.8 mg m^{-2}), indicating subsurface intensification of autotrophic biomass. Compared to reference stations, the eddy exhibited relatively lower nutrient concentrations but generally higher biotic variables, including depth-integrated chlorophyll *a* (25–150 m) and abundances of bacteria, viruses, and pigmented nanoflagellates, although most differences were not statistically significant (Fig. 2). Vertically, within the eddy, nutrient concentrations increased steadily from above to below the vertical core, whereas chlorophyll-*a*, picoeukaryote counts, bacterial and viral abundances decreased over the same interval (all $p < 0.05$) (Fig. 2). Heterotrophic and pigmented nanoflagellate abundances also varied significantly, but primarily between the upper and lower layers. When vertical stratification was examined separately for each locality, these trends remained consistent at the eddy edge (Supporting Information Fig. S1). At the eddy center, vertical patterns persisted for bacteria and viruses, while chlorophyll-*a*, picoeukaryotes, and pigmented nanoflagellate exhibited relatively higher abundances at the vertical core than in the layers above or below, though not all were significant. For nutrients, concentrations still peaked below the vertical core, but the differences between values above and at the vertical core were not statistically significant (Supporting Information Fig. S1). Horizontally, nutrient concentrations were higher at the edge than at the center, while temperature showed the opposite pattern, and these contrasts were significant across all depth layers (Supporting Information Fig. S1). Chlorophyll-*a*, and pigmented nanoflagellate abundances were significantly higher at the edge than at the center above vertical core, but no significant center-edge differences were observed when all depth layers were pooled (Supporting Information Fig. S1).

Alpha diversity and community composition

Microbial alpha-diversity, including richness, Chao1, ACE, and Faith's PD, generally increased with depth, peaking at 150 m for most groups except particle-associated bacteria (Supporting Information Fig. S2). This vertical trend persisted when eddy center and edge samples were analyzed separately (Supporting Information Fig. S2). Horizontally, diversity was consistently higher at the eddy edge than at the center across protists, free-living bacteria, and particle-associated bacteria, and this pattern remained evident within each depth layer, indicating that horizontal variability is robust and not an artifact of vertical aggregation (Supporting Information Fig. S2). Overall, alpha diversity within the eddy exceeded that at reference stations, except for free-living bacteria, which showed no significant difference (Supporting Information Fig. S2).

Our analysis revealed that the eddy imposed a pronounced structuring effect on both protistan and bacterial assemblages (Fig. 3). Protistan communities within the eddy were dominated by Dinophyta, Stramenopiles, Rhizaria, and Ciliophora, together comprising 92.9% of total sequences (Fig. 3a). Dinophyceae were most abundant overall (35.9%), higher at references (38.5%) than within the eddy (35.2%), whereas Pelagophyceae (14.1% vs. 4.0%) and Ciliophora (13.1% vs. 9.1%) were enriched within the eddy (Fig. 3a). Within the eddy, pronounced horizontal contrasts were observed and generally remained consistent across depths: Dinophyceae were consistently higher at the center than at the edge, while Pelagophyceae showed the opposite trend, higher at the edge at and above the vertical core but higher at the center below it (Fig. 3a; Supporting Information Fig. S3a). Vertically, when all within-eddy samples were considered together, Dinophyceae were enriched above the vertical core, whereas Pelagophyceae peaked at the vertical core (Fig. 3a). To test whether these depth-related trends persisted locally, we reanalyzed vertical variation separately for the eddy center and edge. At the center, the overall vertical pattern for Dinophyceae remained consistent, while Pelagophyceae shifted their maximum abundance to below the vertical core. At the edge, the vertical distribution of Dinophyceae reversed (enriched below the core), whereas Pelagophyceae retained their peak at the vertical core (Supporting Information Fig. S3a).

Free-living bacterial communities were dominated by Gammaproteobacteria (Alteromonadales), Cyanobacteria (Synechococcales), Alphaproteobacteria (Rhodobacterales), and Deltaproteobacteria (SAR324), together comprising 90.3% of total sequences (Fig. 3b). Alteromonadales decreased from 41.7% at reference stations to 29.8% within the eddy (Fig. 3b). They were consistently more abundant at the eddy center than at the edge and peaked below the vertical core—a pattern that held across depths and localities (Supporting Information Fig. S3b). Synechococcales exhibited the opposite, being enriched within the eddy (24.2% vs. 5.0% at the reference stations) (Fig. 3b). Horizontally, they were more abundant at the edge than at the center across all depths except below the vertical core, where the trend reversed (center > edge). Vertically, they were more abundant at and above the core than below it (Supporting Information Fig. S3b). Rhodobacterales (*Thalassobius*) showed similar overall abundance inside and outside the eddy but were consistently more concentrated at the center (10.4% vs. 4.1% at the edge) across all depths (Fig. 3b; Supporting Information Fig. S3b). Vertically, they were more abundant below the core (9.3% vs. 5.1%–5.3% at and above the core). This vertical pattern persisted in center samples but reversed at the edge, where their abundance decreased with depth (Fig. 3b; Supporting Information Fig. S3b).

Particle-associated bacterial communities were dominated by Gammaproteobacteria (Alteromonadales), Alphaproteobacteria (Rhodobacterales), and Deltaproteobacteria (Bdellovibrionales), accounting for 93.2% of the total sequences (Fig. 3c). Compared with reference stations, Alteromonadales declined inside the eddy, with low relative abundance at the edge (36.3% vs. 44.5% in the center) and at the vertical core

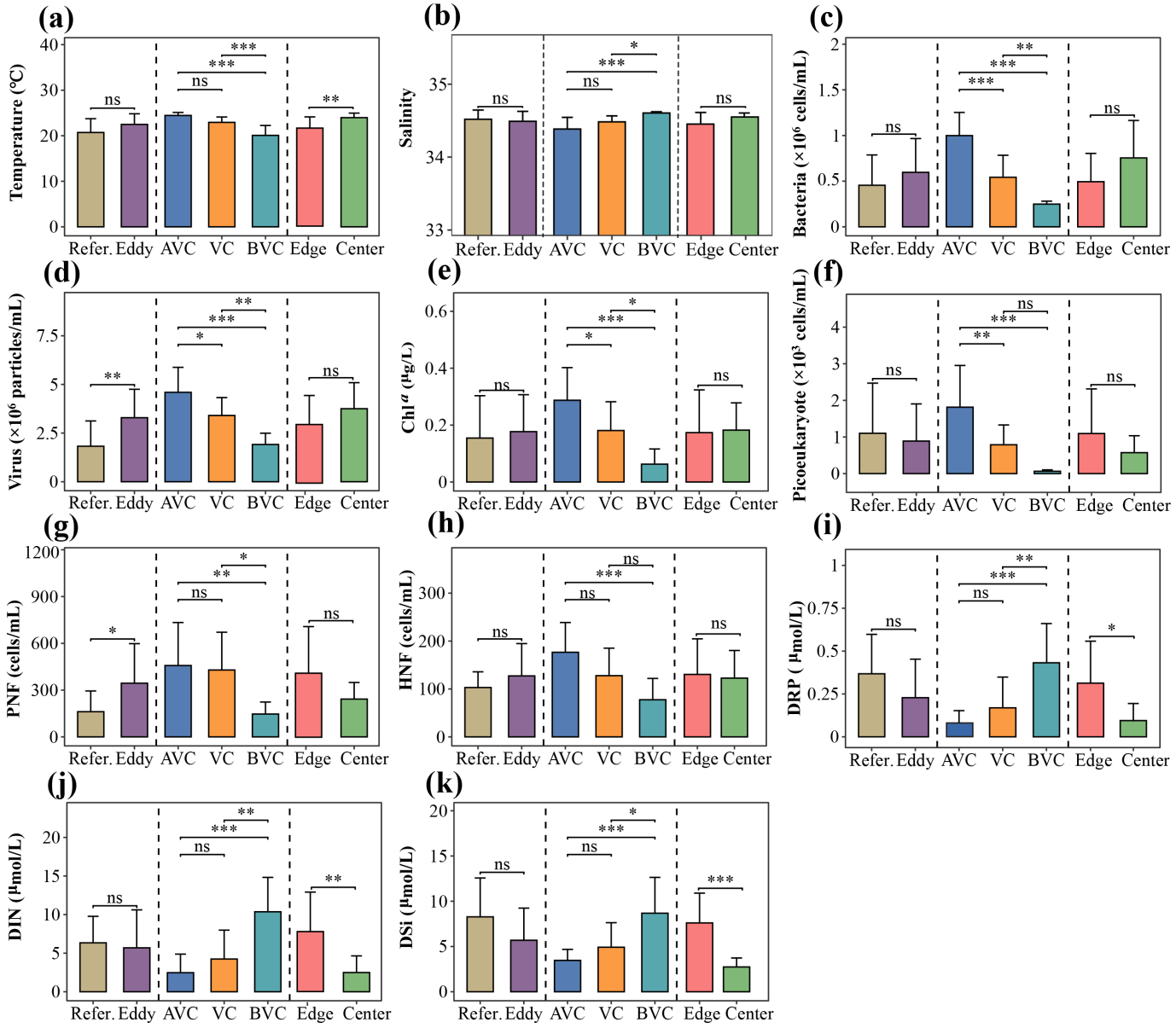

Fig. 2. Bar plots showing the variation of environmental factors among different subgroups. Comparisons are shown between reference stations and eddy stations, among depth layers, and between the eddy center and edge. AVC, above-vertical core; VC, vertical core; BVC, below-vertical core; DRP, dissolved reactive phosphorus; DIN, dissolved inorganic nitrogen; DSi, dissolved inorganic silicate; HNF, heterotrophic nanoflagellates; PNF, pigmented nanoflagellates; Refer., reference stations. Statistical significance is indicated as follows: ns (not significant); ***$p < 0.001$; **$p < 0.01$; *$p < 0.05$.

(32.8% vs. 40.9%–44.9% above and below). These patterns were consistent across depths and localities. In contrast, Rhodobacterales and Bdellovibrionales were enriched inside the eddy (Fig. 3c). Rhodobacterales increased with depth and were more abundant at the center than at the edge across layers and localities (Fig. 3c; Supporting Information Fig. S3c), whereas Bdellovibrionales were less abundant below the vertical core and more abundant at the edge than at the center, patterns that were generally consistent across depths and localities (Fig. 3c; Supporting Information Fig. S3c).

Ecotype-level patterns in chlorophytes and cyanobacteria

Mesoscale eddies have long been recognized to "sort" picoplankton ecotypes by water mass, such as chlorophyte and cyanobacteria. Resolving chlorophytes to species and cyanobacteria to ecotypes, we found that although *Ostreococcus* comprised a minor fraction of the total protistan community, over 99.9% of *Ostreococcus* reads belonged to *O. tauri*. Expressed as a proportion of total protistan reads, *O. tauri* was depleted in the eddy core compared to reference stations (0.97% vs 1.89%), declined from 1.98% above the vertical core

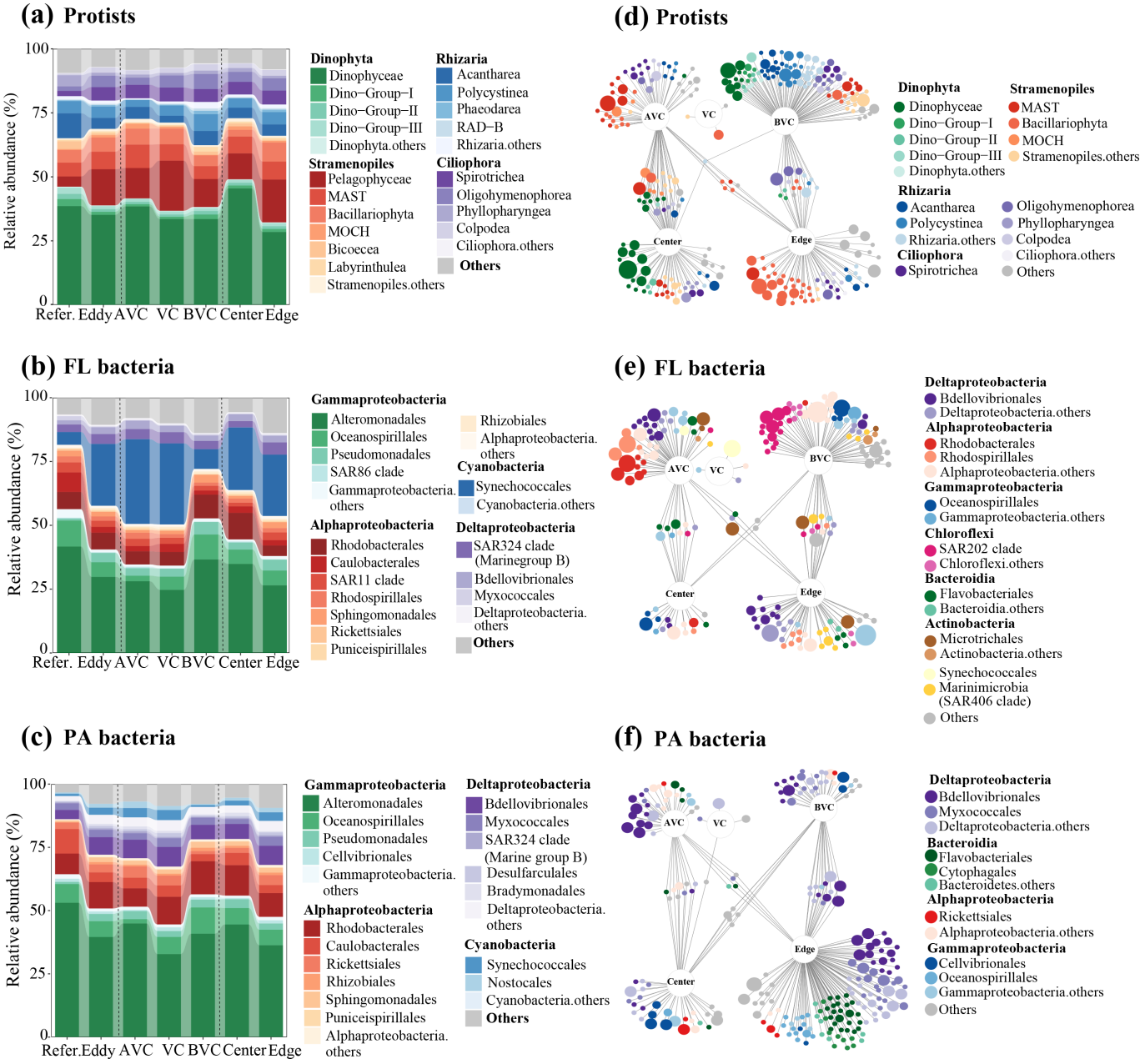

Fig. 3. (**a**–**c**) Alluvial diagrams showing the community composition of (a) protists, (b) free-living bacteria, and (c) particle-associated bacteria at the phylum or class levels across different subgroups. (**d**–**f**) Bipartite networks displaying differential operational taxonomic units (OTUs) in protistan and bacterial communities across vertical and horizontal gradients. Panels show (d) protistan, (e) free-living (FL) bacterial, and (f) particle-associated (PA) bacterial OTUs assigned to classes, orders, or families with significant vertical or horizontal differences, respectively. AVC, above-vertical core; VC, vertical core; BVC, below-vertical core. The AVC, VC, and BVC layers include both center and edge samples to illustrate overall vertical organization within the eddy. Center and edge categories represent horizontally segregated samples combined across all depths.

to 0.05% below it, and peaked at the edge (1.55%) (Fig. 4). In contrast, low-light *Prochlorococcus* MIT9313, expressed as a proportion of total free-living bacterial reads, constituted 16.89% within the eddy compared to 3.15% at reference stations. Its relative contribution was maximal above the vertical core (22.39%), declined below, and was higher at the eddy center (18.28%) than at the edge (15.98%) (Fig. 4). *Synechococcus* CC9902 also enriched within the eddy representing 7.24% of the free-living bacterial reads within the eddy vs. 1.84% at reference stations, peaking at the vertical core (9.77%), and showing comparable distributions at the center (6.17%) and edge (7.93%) (Fig. 4).

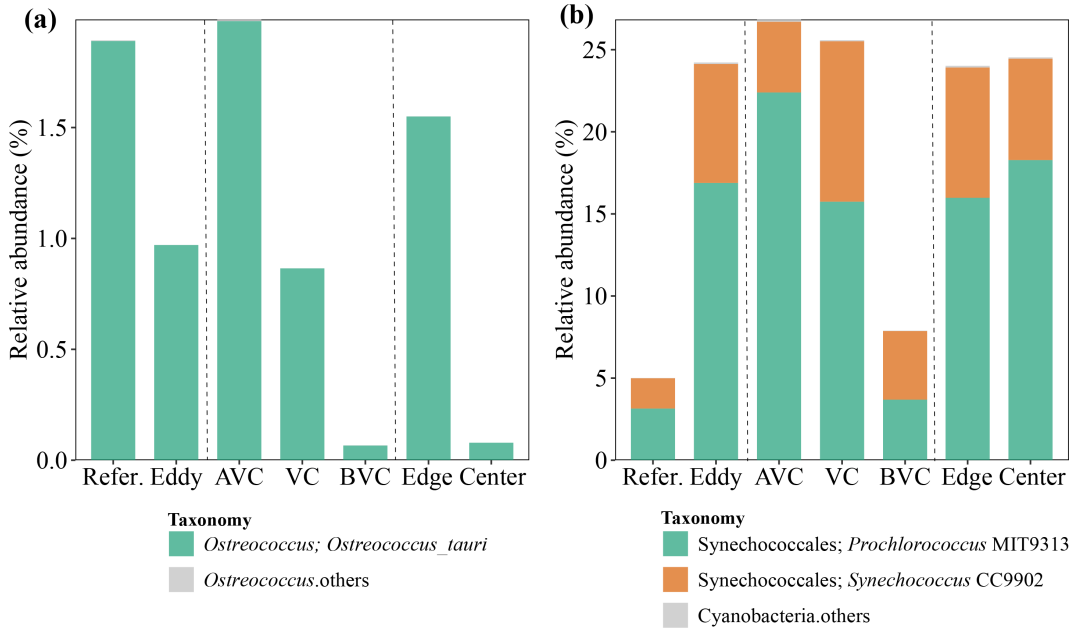

Fig. 4. Relative abundances of *Ostreococcus* and key cyanobacterial ecotypes (*Prochlorococcus* MIT9313 and *Synechococcus* CC9902) across different subgroups. AVC, above-vertical core; VC, vertical core; BVC, below-vertical core.

Vertical and horizontal variations of microbial community within eddy

Our study revealed significant structural differences in microbial communities between the SAE and reference stations, highlighting the eddy's influence on microbial composition. These differences were quantified using the Analysis of Similarities (ANOSIM) (Supporting Information Table S2). Protistan communities exhibited the most pronounced differences between the eddy and reference stations (ANOSIM, $R = 0.518$, $P < 0.001$), followed by particle-associated bacteria ($R = 0.352$, $P < 0.001$) and free-living bacteria ($R = 0.277$, $P < 0.001$). Principal Coordinates Analysis (PCoA) further showed distinct groupings of microbial communities within the eddy, structured by both vertical (above, at, and below the vertical core) and horizontal (center vs. edge) gradients (Fig. 5; Supporting Information Fig. S4). Across all microbial groups, vertical differences in community structure were greater than horizontal differences between the eddy's center and edge (Fig. 5; Supporting Information Fig. S4; Supporting Information Table S2). Within the eddy, vertical variation in community structure was significantly greater than at the reference stations, particularly at the eddy center (Fig. 5). This pattern was observed for both protists and bacteria, with ANOSIM R-values indicating the greatest vertical differentiation at the eddy center for protists ($R = 0.812$) compared to the edge ($R = 0.727$) and reference stations ($R = 0.\ 457$) ($P < 0.001$; Supporting Information Fig. S2). Followed by free-living bacteria (eddy center: $R = 0.722$; eddy edge $R = 0.541$; reference stations $R = 0.547$), then particle-associated Bacteria (eddy center: $R = 0.628$; eddy edge $R = 0.412$; reference stations $R = 0.424$; Fig. 5). For horizontal gradients, protistan communities showed the strongest response, with ANOSIM *R*-values ranging from 0.455 to 0.851 ($P < 0.001$) across depth layers, compared to free-living bacteria ($R = 0.323$–0.492, $P < 0.01$) and particle-associated bacteria ($R = 0.355$–0.755, $P < 0.01$) (Supporting Information Fig. S4; Supporting Information Table S2).

To quantify the SAE's impact, we identified operational taxonomic units that were differentially abundant across vertical (above, at and below vertical core) and horizontal (center vs edge) gradients using Indicator Species Analysis and edgeR. Depth-specific biomarkers numbered 202 protistan operational taxonomic units, 129 free-living bacterial operational taxonomic units, and 96 particle-associated bacterial operational taxonomic units (Supporting Information Fig. S4), collectively contributing 14.65%, 9.75%, and 4.08% of total community sequences, respectively. Center-edge differential operational taxonomic units included 152 protistan, 81 free-living bacterial, and 179 particle-associated bacterial operational taxonomic units (Supporting Information Fig. S4), accounting for 39.35%, 5.63%, and 9.69% of community sequences, respectively. Our study identified distinct microbial biomarkers that corresponded to both vertical (above, at, and below the vertical core) and horizontal (center vs. edge) structural gradients within the SAE. These biomarkers provide insights into the microbial compositional shifts driven by the eddy's unique environmental conditions. Notably, some taxa discussed earlier as ecologically structured by the eddy were also recovered by the differential operational taxonomic units analyses. For example, a non-rare *Ostreococcus* operational taxonomic unit (operational taxonomic unit 8), representing

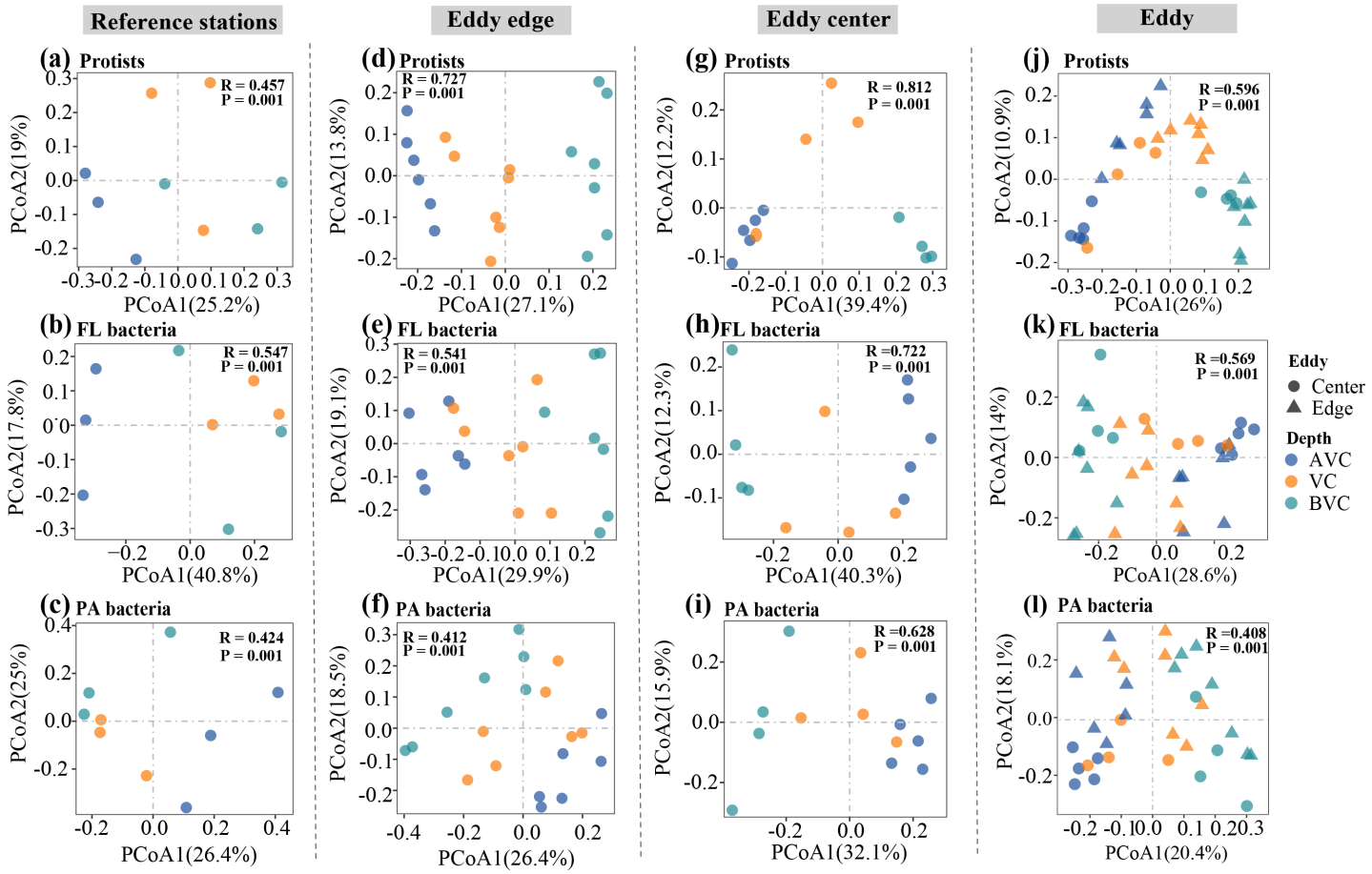

Fig. 5. Principal coordinates analysis (PCoA) plots showing microbial community composition across vertical layers within and outside the subsurface anticyclonic eddy, based on Bray–Curtis dissimilarity. Panels display vertical variation (above-vertical core, vertical core, and below-vertical core) for protists, free-living bacteria, and particle-associated bacteria across reference stations (**a–c**), eddy edge (**d–f**), eddy center (**g–i**), and all eddy (**j–l**) samples combined. AVC, above-vertical core; VC, vertical core; BVC, below-vertical core.

0.97% of total protistan reads, was identified as a shared differential operational taxonomic unit enriched at the eddy edge. In contrast, ecotype-level patterns observed for *Prochlorococcus* and *Synechococcus* were driven primarily by abundant background operational taxonomic units that exhibited consistent depth- and position-related trends, but did not meet the conservative criteria for shared differential operational taxonomic units across statistical methods.

Protistan operational taxonomic units exhibiting vertical differentiation were dominated by Radiolaria (Acantharea, Polycystinea), Ciliophora (Spirotrichea, Oligohymenophorea), and Dinophyta (Dinophyceae, Syndiniales). Together, these groups accounted for 61.39% of vertically differential protistan operational taxonomic units by numbers and 56.36% by relative abundance of vertically differential protistan operational taxonomic units (Fig. 3d). Among free-living bacterial communities, Alphaproteobacteria (Rhodobacterales), Dehalococcoidia (SAR202 clade), and Deltaproteobacteria (Bdellovibrionales) comprised 56.59% of vertically differential operational taxonomic units by numbers and 54.49% of their cumulative relative abundance (Fig. 3e). In particle-associated bacteria, vertically differential operational taxonomic units were dominated by Deltaproteobacteria (notably Bdellovibrionales), representing 57.29% by numbers and 65.42% by relative abundance (Fig. 3f). Differential operational taxonomic units along the center-edge gradient also showed distinct taxonomic affiliations. In protists, Stramenopiles (Bacillariophyta) and Dinophyceae dominated, contributing 53.29% of center-edge differential operational taxonomic units by numbers and 87.18% by cumulative relative abundance (Fig. 3d). In free-living bacteria, Deltaproteobacteria (Bdellovibrionales) and Alphaproteobacteria (Rhodospirillales) accounted for 46.91% of center-edge differential operational taxonomic units by numbers and 35.25% of their cumulative relative abundance (Fig. 3e). In particle-associated bacteria, Bacteroidia (Flavobacteriales) and Deltaproteobacteria (Bdellovibrionales, Myxococcales) dominated, comprising 66.48% by numbers and 59.56% by relative abundance of center-edge differential operational taxonomic units (Fig. 3f). The distinct microbial assemblages

and biomarkers identified here highlight the ecological significance of SAEs in shaping microbial communities.

Factors shaping microbial community within eddy

To evaluate how physicochemical and biological gradients structured microbial communities, we quantified the relationships between environmental variables and protistan, free-living, and particle-associated bacterial assemblages (Fig. 6). Distance-based redundancy analysis (dbRDA) revealed that nutrient (PC1nutrient), temperature–salinity structure ($PC1_{TS}$), chlorophyll-*a*, viruses, and nanoflagellates collectively explained 27%–31% of total community variation across groups (Adj $R^2 = 0.27$–0.31; Fig. 6). For protists, community structure was primarily shaped by bacterial and viral abundances (individual contributions = 41.17%, $p < 0.001$), followed by the nutrient gradient (22.09%, $p < 0.001$), and temperature-salinity conditions (20.28%, $p < 0.001$; Fig. 6a). In free-living bacteria, viral, nutrient, and temperature-salinity variables were the dominant explanatory factors (19.28%–29.77%, $p < 0.01$), with nanoflagellate abundance also contributing significantly (Fig. 6b). Particle-associated bacterial communities were similarly structured by these gradients, with nanoflagellates and nutrients contributing comparably (25.41% and 25.37%, respectively, $p < 0.01$; Fig. 6c), underscoring the strong coupling of particulate microbial niches to both resource availability and trophic interactions. Across all microbial groups, chlorophyll-*a* made a minor contribution to the total variance. Mantel test between environmental factors and community variations showed the same result (Supporting Information Table S3). In addition, protistan and bacterial community structures were strongly correlated. Mantel analyses revealed strong associations between protistan and free-living bacterial communities ($r = 0.830$, $p < 0.001$) as well as particle-associated bacterial communities ($r = 0.733$, $p < 0.001$). These relationships remained significant after controlling for depth (partial Mantel $r = 0.721$ and 0.661, respectively; $p < 0.001$). Collectively, these analyses demonstrate that microbial community assembly within the subsurface anticyclonic eddy reflects the combined influence of nutrient availability, water-mass structure, biological interactions (bacteria, viruses, and nanoflagellates), and coordinated turnover between protistan and bacterial communities.

Protists–bacteria co-occurrence network

To elucidate potential interactions among active microbial taxa within the SAE, we constructed a protist–bacteria co-occurrence network. The resulting network comprised 1031 nodes (362 protist, 287 free-living bacterial, 382 particle-associated bacterial taxa) and 14,181 edges, of which 10,614 were positive and 3567 negative (Fig. 7). Cross-domain links were abundant: 2458 protist–free-living bacterial and 2263 protist–particle-associated bacterial edges, alongside 2552 protist–protist, 1561 free-living–free-living, 2724 particle-associated–particle-associated, and 2623 free-living–particle-associated bacterial connections. Network topology metrics (average path length, clustering coefficient) significantly exceeded those of degree-preserving randomized networks (Supporting Information Table S4), consistent with a "small-world" architecture, while a power-law degree distribution confirmed a scale-free, non-random structure (Supporting Information Table S4).

Modularity analysis partitioned the network into three major modules, collectively containing ~70% of nodes, each mapping to specific vertical or horizontal SAE niches (ternary plot, Fig. 7). Module I (above-core waters) enriched in free-living Alphaproteobacteria (Rhodobacterales), particle-associated Deltaproteobacteria (Bdellovibrionales), and Stramenopiles (MAST, diatoms), reflecting high-light conditions. Module II (below-core waters) dominated by free-living Chloroflexi (SAR202), particle-associated Deltaproteobacteria, and protists—including Rhizaria (Polycystinea), Ciliophora

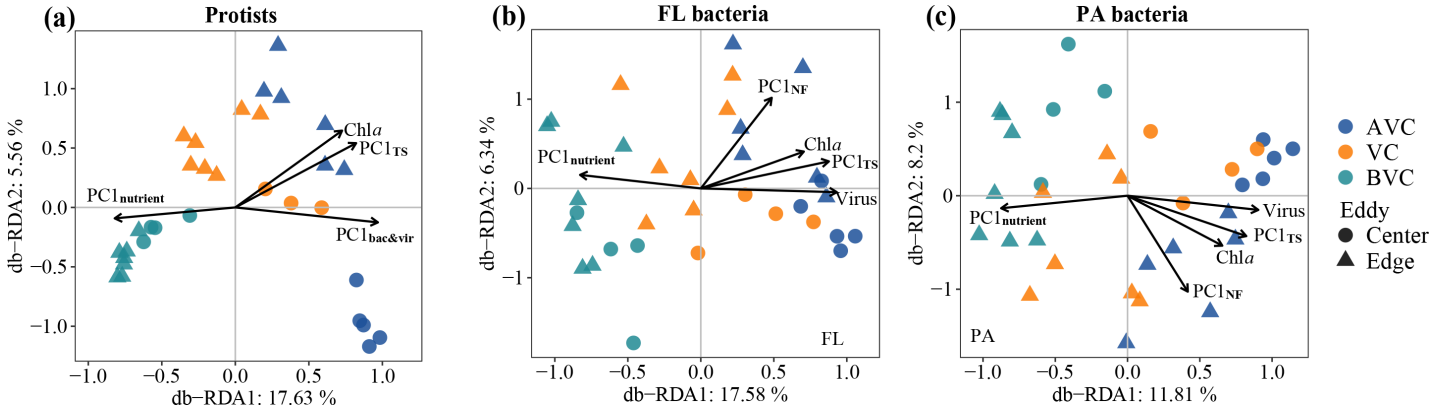

Fig. 6. Distance-based redundancy analysis (dbRDA) based on Bray–Curtis dissimilarities showing the relationships between environmental factors and microbial communities for (**a**) protists, (**b**) free-living (FL) bacteria, and (**c**) particle-associated (PA) bacteria. AVC, above-vertical core; VC, vertical core; BVC, below-vertical core. To minimize collinearity among predictors, environmental variables were summarized as principal components: $PC1_{nutrient}$, nutrient gradient; $PC1_{TS}$, temperature-salinity structure; $PC1_{bac\&vir}$, bacterial and viral distribution; $PC1_{NF}$: pigmented and heterotrophic nanoflagellates.

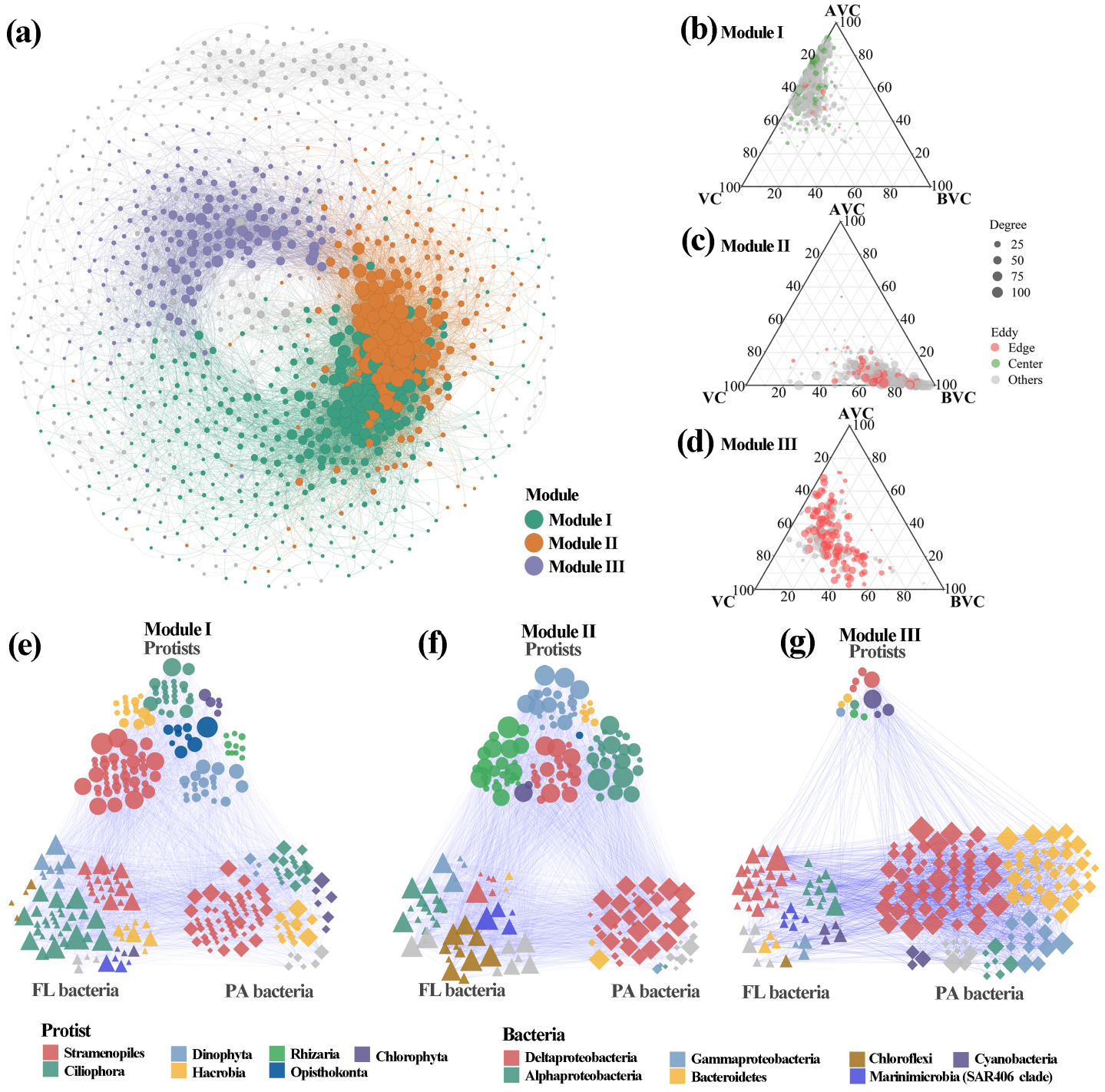

Fig. 7. (**a**) Co-occurrence network of protistan and bacterial communities within the subsurface anticyclonic eddy. Three topological modules (I–III) are identified and color-coded. (**b–d**) Ternary plots showing the proportional distribution of individual operational taxonomic units across three depth layers: above the vertical core (AVC), vertical core (VC), and below the vertical core (BVC). Each axis represents the relative contribution (%) of an operational taxonomic unit to one depth layer, with proportions summing to 100% across the three layers. Point position indicates depth affinity, point color denotes sampling location (eddy center, eddy edge, or others), and point size ("degree") represents the number of connections of each node within the corresponding co-occurrence module. (**e–g**) Sub-network visualizations of modules I–III, illustrating the direction and strength of cross-domain associations. Nodes represent individual operational taxonomic units, with circles for protists, triangles for free-living bacteria, and squares for particle-associated bacteria; node size is proportional to the degree (number of connections).

(Scuticociliatia), and Syndiniales—consistent with low-light microhabitats (Fig. 7). Module III (edge waters) characterized by particle-associated Deltaproteobacteria (Myxococcales, Bdellovibrionales) and Bacteroidetes (Flavobacteriales), indicative of enhanced mixing and nutrient inputs (Fig. 7). Key hub taxa (highest degree and betweenness centrality) included Stramenopiles, free-living Actinobacteria, and particle-associated Deltaproteobacteria, underscoring their pivotal role in linking phototrophic and heterotrophic assemblages across the SAE's vertical and horizontal microhabitats.

Discussion

Vertical and horizontal structuring of microbial assemblages in the SAE

Mesoscale eddies isolate and transport distinct water masses, often shaping microbial communities distinct markedly from surrounding waters (Chelton et al. 2011; Nelson et al. 2014). Similar studies of Western Boundary Current fronts have shown that these energetic boundaries host assemblages distinct from both adjacent productive and oligotrophic provinces, with elevated diatom and dinoflagellate biomass alongside peaks in appendicularians and rhizarians (Mangolte et al. 2022, 2023). In our subsurface anticyclonic eddy, the velocity core at ~ 90 m (max ~ 0.46 m s^{-1}) was bounded by two shear layers (Ri < 0.25; 3.5-fold increase in diapycnal diffusivity; Qi et al. 2022), defining three physical strata that are above vertical core, vertical core, and below vertical core. This stratification was mirrored in microbial assemblages (Fig. 5). PCoA and ANOSIM revealed stronger vertical turnover within the SAE than at reference sites (Fig. 5; Supporting Information Table S2). The euphotic depth (Z_{eu}) deepened progressively from the reference waters (107.9 m) to the eddy edge (117.9 m) and center (124.5 m), consistent with the anticyclonic downwelling signature (Wang et al. 2023). Consequently, the 75 m and 100 m samples were within or at the base of the euphotic zone, whereas the 150 m samples were below it at all habitats. Above the core, protistan communities were dominated by autotrophic and mixotrophic lineages, raphid-pennate and mediophycean diatoms, Spirotrichea, and Dinophycea, coinciding with elevated chlorophyll-*a* and optimal light–nutrient conditions at the edge but significant lower nutrients conditions at the center (Pierce and Turner 1992). This pattern aligns with recent observations of increased ciliate abundance in anticyclonic eddies (Beatty et al. 2025). Below the core, heterotrophs and parasites (Syndiniales, Radiolaria, Scuticociliatia) prevailed, reflecting low-light conditions and reliance on deep-water organic pools (Sun et al. 2024). Depth-differentiated protist operational taxonomic units (14.7% of total; identified by Indicspecies and edgeR) confirm discrete niche partitioning along gradients of irradiance, temperature, and nutrient availability. This optical structure reinforces the observed biological zonation that phototrophic and mixotrophic lineages were largely confined to layers above the vertical core, whereas heterotrophic and parasitic assemblages dominating below the euphotic boundary. These patterns are further supported by dbRDA and Mantel analyses, which showed that protistan communities were primarily structured by temperature, nutrient availability, and biotic factors such as viral and bacterial abundances and chlorophyll-*a* concentrations (Fig. 6; Supporting Information Table S3). In addition, protistan and bacterial community structures covaried strongly, indicating coordinated turnover across trophic levels. Protistan assemblages were tightly correlated with both free-living and particle-associated bacterial communities (Mantel $r = 0.830$ and 0.733, respectively; both $p < 0.001$), and these relationships remained significant after controlling for depth (partial Mantel $r = 0.721$ and 0.661; both $p < 0.001$). This concordance likely reflects the combined influence of shared environmental filtering and direct or indirect biotic interactions, including grazing, parasitism, and protist-derived organic matter that shapes bacterial niches. Because bulk chlorophyll-*a* integrates phytoplankton biomass but not producer identity or DOM quality, it may explain comparatively little bacterial variation even when protistan composition changes markedly. Correlations between differentially distributed assemblages and environmental factors further revealed that vertically segregated protistan lineages are tightly coupled to biogeochemical gradients (Supporting Information Fig. S6). Specifically, Spirotrichea, Oligohymenophorea (mainly Scuticociliatia), and Radiolaria (mainly Acantharea and Polycystinea), showed strong associations with bacterial and viral abundances, temperature, dissolved inorganic nutrients, and chlorophyll-*a* ($r = 0.18$–0.66, all $p < 0.001$; Supporting Information Fig. S6), suggesting that physiochemical structures and biological interactions jointly modulate their distribution.

Free-living bacteria exhibited similar vertical trends. Rhodobacterales peaked above the vertical core, whereas the SAR202 clade dominated below it. Mantel tests showed that Bdellovibrionales and Rhodobacterales were strongly correlated with nutrients and viral variables ($r = 0.20$–0.39, $p < 0.01$), indicating that both bottom-up nutrient supply and viral top-down regulation influence free-living bacterial assembly. The SAR202 clade was similarly linked to dissolved inorganic nitrogen and viral abundance ($r = 0.24$–0.50, $p < 0.01$), suggesting that deep-water bacterial turnover is tightly coupled to nutrient cycling and viral lysis. In contrast, particle-associated bacteria displayed minimal vertical differentiation (4.1% depth-differentiated operational taxonomic units), implying that shear-driven particle mixing homogenizes their distribution within the eddy.

Horizontal (center–edge) contrasts were equally pronounced. Protists exhibited the strongest horizontal segregation (39% of operational taxonomic units; ANOSIM $R = 0.455$–0.851 across depths, $P < 0.001$; Supporting Information Fig. S4). Bacillariophyta peaked at the edge, likely fueled by submesoscale upwelling and lateral nutrient inputs, whereas Dinophyceae dominated the interior, reflecting mixotrophic

resilience in oligotrophic cores (Gleich et al. 2024). Mantel correlations based on communities of differentially distributed operational taxonomic units supported these ecological interpretations that Bacillariophyta were strongly associated with dissolved inorganic silicate and nitrogen, as well as bacterial and viral abundances ($r = 0.20$–0.61, $p < 0.02$; Supporting Information Fig. S6), consistent with their dependence on nutrient availability (Romero et al. 2016;), taxa-specific coupling with heterotrophic bacteria via phytoplankton-derived dissolved organic matter (e.g., diatom–Rhodobacterales interactions; Amin et al. 2012), and viral regulation (Pelusi et al. 2021) in productive edge waters. In contrast, Dinophyceae showed strong correlations with bacterial abundance ($r = 0.553$, $p < 0.001$) and dissolved nutrients ($r = 0.565$–0.634, $p < 0.001$; Supporting Information Fig. S6), supporting a mechanistic explanation in which dinoflagellate activity persists under low ambient nutrients through bacterivory or uptake of regenerated nitrogen and phosphorus, hallmarks of mixotrophic nutrition (Jeong et al. 2010; Stoecker et al. 2017). Thus, the observed Dinophyceae enrichment represents not merely a taxonomic shift but a functional response to stratified, resource-limited conditions in eddy center. Together, these relationships indicate that the contrasting diatom–dinoflagellate distributions between the eddy edge and center reflect a shift from new production driven by nutrient entrainment to a recycled, mixotrophy-dominated productivity regime within the eddy center.

Free-living bacteria showed moderate horizontal structuring ($R = 0.323$–0.492, $P < 0.01$), whereas particle-associated bacteria were even more differentiated ($R = 0.355$–0.755, $P < 0.01$). Among particle-associated taxa, predatory Bdellovibrionales and Myxococcales, along with the OM27 clade, critical players in the degradation of dissolved organic matter (Ezzedine et al. 2022; Hungate et al. 2021), were enriched at the edge, where elevated particle flux and nutrient availability create localized biogeochemical hotspots. Mantel analyses further confirmed that Bdellovibrionales and Myxococcales correlated with viral abundances ($r = 0.22$–0.30, $p < 0.01$; Supporting Information Fig. S6), suggesting that predation and viral lysis jointly regulate particle-associated bacterial activity, stimulating organic-matter remineralization and nutrient recycling along the eddy edge (Ezzedine et al. 2022; Hungate et al. 2021).

Our use of rRNA likely accentuates taxa with high ribosome content, emphasizing active copiotrophs (e.g., *Alteromonadales*) and metabolically active phototrophs or mixotrophs, while potentially inflating their proportional representation relative to rDNA inventories (Blazewicz et al. 2013; Giner et al. 2020). This pattern explains the elevated rRNA signal of *Alteromonadales* in the free-living fraction (Fig. 3): copiotrophs rapidly upregulate ribosomes under nutrient supply, so their rRNA shares exceed what rDNA would suggest. For dinoflagellates, 18S rDNA copy number varies by orders of magnitude among species; although rRNA abundance does not directly mirror gene copy number, ribosome content scales with cell size and growth state (Ruvindy et al. 2023). Consequently, rRNA-based data may overrepresent large or fast-growing dinoflagellates relative to cell counts. We therefore interpret rRNA proportions as indicators of potential metabolic activity rather than absolute abundance, highlighting how light–nutrient regimes modulate microbial responsiveness within the eddy.

Although our sampling strategy captured the principal hydrographic and ecological transitions of the subsurface anticyclonic eddy, the vertical resolution (surface, 75, 100, and 150 m) inevitably limits detection of finer-scale gradients, particularly within the upper 25–50 m layer, where isopycnal doming is most pronounced. Previous studies have shown that microbial composition, chlorophyll-*a*, and nutrient distributions can shift sharply within these shallow transition zones (Sasai et al. 2006; Spingys et al. 2021). The absence of samples from this layer may therefore underestimate the steepness of biological and chemical gradients within the eddy. Nonetheless, the strong vertical turnover observed between 75 and 150 m demonstrates that our sampling depth effectively captured the core stratification structuring microbial assemblages. Future high-resolution profiling (e.g., 10–20 m intervals) will help resolve these microscale transitions and better constrain biogeochemical fluxes across the eddy's upper interface.

Enhanced alpha-diversity in SAE

Mesoscale eddies exert contrasting influences on microbial diversity. Cyclonic eddies typically enrich protist richness through nutrient injection, whereas surface-intensifying anticyclonic eddies often homogenize communities and reduce diversity (Chen et al. 2015; Gleich et al. 2024). In contrast, our long-lived SAE exhibited significantly elevated alpha-diversity for both protists and particle-associated bacteria compared to adjacent reference waters (Fig. 2). This enhancement reflects the SAE's distinctive lens-shaped hydrography and internal biogeochemical gradients, which generate multiple coexisting microhabitats. At the eddy edge, submesoscale upwelling delivers pulses of nitrate and phosphate that fuel localized phytoplankton blooms and elevated chlorophyll-*a* concentrations (Wang et al. 2018; Zhou et al. 2013), coinciding with a surge in Bacillariophyta operational taxonomic units and peak protist richness. For particle-associated bacteria, alpha-diversity gains within the eddy are likely linked to the greater availability of particulate organic matter at the edge, which offers diverse surfaces and substrates for metabolic specialization and niche partitioning (Chen et al. 2024). By contrast, free-living bacterial alpha-diversity showed only marginal increases within the SAE, which may reflect the relatively uniform and low concentrations of dissolved organic substrates throughout the eddy lens. Studies in the South China Sea that did not distinguish free-living from particle-associated fractions likely underestimated this particle-associated specific diversity enhancement (Sun et al. 2021). Critically, our high-resolution sampling design—targeting both center and edge stations at multiple depths—was

essential for resolving the fine-scale gradients underpinning alpha-diversity peaks. Previous surveys employing coarser station grids lacked the spatial resolution required to detect these microhabitat-driven diversity patterns in long-lived subsurface eddies. In summary, the unexpectedly high protist and particle-associated bacterial richness within the SAE underscores how subsurface anticyclonic dynamics shape diverse ecological niches. These findings highlight the importance of depth- and feature-specific sampling for accurately assessing microbial diversity patterns in complex mesoscale structures.

Ecotype-level niche partitioning of chlorophytes and cyanobacteria

Mesoscale eddies impose sharp light–nutrient gradients that act as ecological filters for microbial ecotypes (Sheyn et al. 2025). Within our subsurface anticyclonic eddy, these filters produced mirrored distributions of the high-light chlorophyte *O. tauri* and the low-light picocyanobacterium *Prochlorococcus* MIT9313. *Ostreococcus* comprises distinct ecotypes with contrasting light–nutrient adaptations (Demir-Hilton et al. 2011; Clayton et al. 2017). High-light clades dominate sunlit surface waters, while low-light lineages persist deeper in oligotrophic layers. Fine-scale surveys at the Kuroshio Front have even distinguished "coastal/mesotrophic" (OI) vs. "open-ocean" (OII) *Ostreococcus* ecotypes tied to specific water masses (Clayton et al. 2017), with similar biogeographical partitioning across the North Pacific (Simmons et al. 2016). In our study, the high-light specialist *O. tauri* was markedly depleted in the SAE relative to reference sites, declined steadily from above to below the vertical core, and peaked at the eddy edge. These patterns indicate that high-light ecotypes can withstand the intensified mixing but require sufficient irradiance, whereas neither high- nor low-light lineages thrive in the dark, nutrient-poor interior.

In parallel, *Prochlorococcus* MIT9313, a low-light–adapted LL ecotype, was significantly enriched within the ACE lens. MIT9313 reached its maximum just above the vertical core (75 m), decreased toward 150 m, and exhibited higher abundance in the eddy center than at the edge (Fig. 4). Previous work by Sheyn et al. (2025) documented enrichment of high-light *Prochlorococcus* clades (HLI/HLII) in cyclonic eddies; our results extend this paradigm by demonstrating that ACE cores act as refugia for LL-adapted lineages. The decline of each ecotype outside its preferred depth, above the vertical core, underscores light availability and nutrient supply as the principal niche axes in subsurface anticyclonic eddies. By resolving these fine-scale, ecotype-specific patterns, our study shows that SAEs function as microscale biogeographical filters, partitioning microbial diversity across the light–nutrient continuum.

Protist–bacteria co-occurrence network

The co-occurrence network revealed a modular architecture tightly aligned with the SAE's physical gradients, indicating that microbial interactions are highly sensitive to both depth and horizontal position. We identified three major modules (Fig. 7). Module I (above vertical core) enriched in Stramenopiles (MAST clades, diatoms), Spirotrichea ciliates, Dinophycea, Bdellovibrionales, and Flavobacteriales, reflecting interactions of phototrophic, mixotrophic, and heterotrophic interactions in the light layer. Module II (below vertical core, 150 m) dominated by Polycystinea (Radiolaria), Scuticociliatia, Syndiniales, SAR202, Bdellovibrionales, and Myxococcales, indicative of predator–prey and parasitic associations under low-light conditions. Module III (edge waters) characterized by particle-associated Bdellovibrionales, Myxococcales, and Flavobacteriales, signifying predatory and copiotrophic bacterial niches at the eddy edge where particle and nutrient concentrations peak. Keystone taxa—identified by high betweenness and degree centrality—include Stramenopiles, free-living Actinobacteria, and particle-associated Deltaproteobacteria, each acting as hubs connecting modules and maintaining network cohesion. While correlation networks cannot prove direct interactions, the spatially coherent modules suggest a valuable framework for exploring potential ecological relationships within the SAE.

Ecosystem and biogeochemical implications

Depth-integrated chlorophyll-*a* between 25 and 150 m was higher inside the eddy (19.7 mg m^{-2}) than at reference stations (18.2 mg m^{-2}), with elevated values at both the center (20.8 mg m^{-2}) and edge (19.1 mg m^{-2}) (Fig. 2l). This pattern indicates that, despite overall nutrient depletion in the eddy core, subsurface biomass and primary production remained enhanced relative to surrounding waters (He et al. 2021; Wang et al. 2023). The elevated integrated chlorophyll-*a* reflects the combined influence of deepened light penetration and efficient internal nutrient recycling, with distinct mechanisms operating across eddy zones: submesoscale upwelling at the edge supplies nutrients that stimulate diatom growth, whereas recycled nutrient pathways in the center sustain mixotrophic and heterotrophic activity within the deepened euphotic layer (Supporting Information Fig. S7). Collectively, these findings indicate that the subsurface anticyclonic eddy functions not only as a physical trapping feature but also as a localized biogeochemical reactor, coupling light-nutrient-driven production with microbial recycling to sustain productivity in oligotrophic waters.

Author Contributions

Ping Sun: Writing – review and editing, writing – original draft, visualization, formal analysis, data curation, conceptualization. Ying Wang: Writing – original draft, formal analysis, data curation. Zhaomin Han: Writing – original draft, investigation, data curation. Lei Wang: Writing – review and editing. Peng Cheng: Writing – review and editing, data curation. Dapeng Xu: Writing – review and editing, writing – original draft, formal analysis, conceptualization, funding acquisition. Bangqin Huang: Writing – review and editing, conceptualization, funding acquisition.

Acknowledgments

Data and sample were collected onboard R/V "Dongfanghong 3" implementing the open research cruise NORC2021-05 supported by NSFC Shiptime Sharing Project (project number: 42049905). We thank Dr. Yuyuan Xie (College of Marine Science, University of South Florida, St. Petersburg, FL, USA) for assistance with calculating the euphotic zone depth. This work was supported by the National Natural Science Foundation of China (42130401, 42276095).

Conflicts of Interest

None declared.

Data Availability Statement

All the sequencing reads for 18S and 16S rRNA genes from this study have been deposited in the public NCBI Sequence Read Archive (SRA) database under BioProject accession number PRJNA1150504 (https://www.ncbi.nlm.nih.gov/bioproject/PRJNA1150504/).

References

Amin, S. A., M. S. Parker, and E. V. Armbrust. 2012. "Interactions Between Diatoms and Bacteria." *Microbiology and Molecular Biology Reviews* 76: 667–684. https://doi.org/10.1128/mmbr.00007-12.

Apprill, A., S. McNally, R. Parsons, and L. Weber. 2015. "Minor Revision to V4 Region SSU rRNA 806R Gene Primer Greatly Increases Detection of SAR11 Bacterioplankton." *Aquatic Microbial Ecology* 75: 129–137. https://doi.org/10.3354/ame01753.

Bastian, M., S. Heymann, and M. Jacomy. 2009. "Gephi: An Open Source Software for Exploring and Manipulating Networks, v0.9.5." In Proceedings of the International AAAI Conference on Web and Social Media, vol. 3, 361–362. AAAI Press. https://doi.org/10.1609/icwsm.v3i1.13937.

Beatty, J. L., B. P. Stewart, L. Y. Mesrop, E. F. DeLong, D. M. Karl, and D. A. Caron. 2025. "Eddy Dipole Differentially Influences Particle-Associated and Water Column Protistan Community Composition." *Limnology and Oceanography* 70: 817–832. https://doi.org/10.1002/lno.12785.

Blazewicz, S. J., R. L. Barnard, R. A. Daly, and M. K. Firestone. 2013. "Evaluating rRNA as an Indicator of Microbial Activity in Environmental Communities: Limitations and Uses." *The ISME Journal* 7: 2061–2068. https://doi.org/10.1038/ismej.2013.102.

Caporaso, J. G., J. Kuczynski, J. Stombaugh, et al. 2010. "QIIME Allows Analysis of Highthroughput Community Sequencing Data." *Nature Methods* 7, no. 5: 335–336. https://doi.org/10.1038/nmeth.f.303.

Carton, X. 2001. "Hydrodynamical Modeling of Oceanic Vortices." *Surveys in Geophysics* 22, no. 3: 179–263. https://doi.org/10.1023/A:1013779219578.

Chelton, D. B., M. G. Schlax, and R. M. Samelson. 2011. "Global Observations of Nonlinear Mesoscale Eddies." *Progress in Oceanography* 91, no. 2: 167–216. https://doi.org/10.3390/v16060937.

Chen, P. W., M. Olivia, G. Gong, S. Jan, and A. Tsai. 2024. "Viral Dynamics in the Tropical Pacific Ocean: A Comparison Between Within and Outside a Warm Eddy." *Viruses* 16, no. 6: 937. https://doi.org/10.3390/v16060937.

Chen, Y. L., H.-Y. Chen, S. Jan, Y.-H. Lin, T.-H. Kuo, and J.-J. Hung. 2015. "Biologically Active Warm-Core Anticyclonic Eddies in the Marginal Seas of the Western Pacific Ocean." *Deep Sea Research Part I* 106: 68–84. https://doi.org/10.1016/j.dsr.2015.10.006.

Clayton, S., Y.-C. Lin, M. J. Follows, and A. Z. Worden. 2017. "Co-Existence of Distinct *Ostreococcus* Ecotypes at an Oceanic Front." *Limnology and Oceanography* 62, no. 1: 75–88. https://doi.org/10.1002/lno.10373.

Dell'Anno, A., and C. Corinaldesi. 2004. "Degradation and Turnover of Extracellular DNA in Marine Sediments: Ecological and Methodological Considerations." *Applied and Environmental Microbiology* 70, no. 7: 4384–4386. https://doi.org/10.1128/AEM.70.7.4384-4386.2004.

Demir-Hilton, E., S. Sudek, M. L. Cuvelier, C. L. Gentemann, J. P. Zehr, and A. Z. Worden. 2011. "Global Distribution Patterns of Distinct Clades of the Photosynthetic Picoeukaryote *Ostreococcus*." *The ISME Journal* 5, no. 7: 1095–1107. https://doi.org/10.1038/ismej.2010.209.

Du, C., Z. Liu, M. Dai, et al. 2013. "Impact of the Kuroshio Intrusion on the Nutrient Inventory in the Upper Northern South China Sea: Insights From an Isopycnal Mixing Model." *Biogeosciences* 10: 6419–6432. https://doi.org/10.5194/bg-10-6419-2013.

Dugan, J. P., R. P. Mied, P. C. Mignerey, and A. F. Schuetz. 1982. "Compact, Intrathermocline Eddies in the Sargasso Sea." *Journal of Geophysical Research: Oceans* 87: 385–393. https://doi.org/10.1029/JC087iC01p00385.

Edgar, R. C. 2013. "UPARSE: Highly Accurate OTU Sequences From Microbial Amplicon Reads." *Nature Methods* 10: 996–998. https://doi.org/10.1038/nmeth.2604.

Ezzedine, J. A., A. Janicot, S. Rasconi, I. Domaizon, and S. Jacquet. 2022. "Short-Term Dynamics of Bdellovibrio and like Organisms in Lake Geneva in Response to a Simulated Climatic Extreme Event." *Microbial Ecology* 84: 717–729. https://doi.org/10.1007/s00248-021-01875-9.

Giner, C. R., M. C. Pernice, V. Balagué, et al. 2020. "Marked Changes in Diversity and Relative Activity of Picoeukaryotes With Depth in the World Ocean." *The ISME Journal* 14: 437–449. https://doi.org/10.1038/s41396-019-0506-9.

Gleich, S. J., S. K. Hu, A. I. Krinos, and D. A. Caron. 2024. "Protistan Community Composition and Metabolism in the North Pacific Subtropical Gyre: Influences of Mesoscale Eddies and Depth." *Environmental Microbiology* 26, no. 1: e16556. https://doi.org/10.1111/1462-2920.16556.

Guillou, L., D. Bachar, S. Audic, et al. 2013. "The Protist Ribosomal Reference Database, No. PR2: A Catalog of Unicellular Eukaryote Small Sub-Unit rRNA Sequences With Curated Taxonomy." *Nucleic Acids Research* 41: D597–D604. https://doi.org/10.1093/nar/gks1160.

He, Q., H. Zhan, S. Cai, and W. Zhan. 2021. "Eddy-Induced Near-Surface Chlorophyll Anomalies in the Subtropical Gyres: Biomass or Physiology?" *Geophysical Research Letters* 48: e2020GL091975. https://doi.org/10.1029/2020GL091975.

Hungate, B. A., J. C. Marks, M. E. Power, et al. 2021. "The Functional Significance of Bacterial Predators." *MBio* 12, no. 2: e00466-21. https://doi.org/10.1128/mbio.00466-21.

Jeong, H. J., Y. D. Yoo, J. S. Kim, K. A. Seong, N. S. Kang, and T. H. Kim. 2010. "Growth, Feeding and Ecological Roles of the Mixotrophic and Heterotrophic Dinoflagellates in Marine Planktonic Food Webs." *Ocean Science Journal* 45: 65–91. https://doi.org/10.1007/s12601-010-0007-2.

Lee, Z., A. Weidemann, J. Kindle, R. Arnone, K. L. Carder, and C. Davis. 2007. "Euphotic Zone Depth: Its Derivation and Implication to Ocean-Color Remote Sensing." *Journal of Geophysical Research. Oceans* 112: 2006JC003802. https://doi.org/10.1029/2006JC003802.

Malmstrom, R. R., A. Coe, G. C. Kettler, et al. 2010. "Temporal Dynamics of *Prochlorococcus* Ecotypes in the Atlantic and Pacific Oceans." *The ISME Journal* 4, no. 10: 1252–1264. https://doi.org/10.1038/ismej.2010.60.

Mangolte, I., M. Lévy, C. Haëck, and M. D. Ohman. 2023. "Sub-Frontal Niches of Plankton Communities Driven by Transport and Trophic Interactions at Ocean Fronts." *Biogeosciences* 20, no. 15: 3273–3299. https://doi.org/10.5194/bg-20-3273-2023.

Mangolte, I., S. Lévy, S. Dutkiewicz, S. Clayton, and O. Jahn. 2022. "Plankton Community Response to Fronts: Winners and Losers." *Journal of Plankton Research* 44, no. 2: 241–258. https://doi.org/10.1093/plankt/fbac010.

McGillicuddy, D. J., R. Johnson, D. A. Siegel, A. F. Michaels, N. R. Bates, and A. H. Knap. 1999. "Mesoscale Variations of Biogeochemical Properties in the Sargasso Sea." *Journal of Geophysical Research. Oceans* 104, no. C6: 13381–13394. https://doi.org/10.1029/1999JC900021.

McWilliams, J. C. 1985. "Submesoscale, Coherent Vortices in the Ocean." *Reviews of Geophysics* 23: 165–182. https://doi.org/10.1029/RG023i002p00165.

Meunier, T., M. Tenreiro, E. Pallàs-Sanz, et al. 2018. "Intrathermocline Eddies Embedded Within an Anticyclonic Vortex Ring." *Geophysical Research Letters* 45, no. 15: 7624–7633. https://doi.org/10.1029/2018GL077527.

Moore, L. R., and S. W. Chisholm. 1999. "Photophysiology of the Marine Cyanobacterium *Prochlorococcus*: Ecotypic Differences Among Cultured Isolates." *Limnology and Oceanography* 44, no. 3: 628–638. https://doi.org/10.4319/lo.1999.44.3.0628.

Nan, F., H. Xue, P. Xiu, F. Chai, M. Shi, and P. Guo. 2011. "Oceanic Eddy Formation and Propagation Southwest of Taiwan." *Journal of Geophysical Research* 116: C12045. https://doi.org/10.1029/2011JC007386.

Nan, F., F. Yu, C. Wei, Q. Ren, and C. Fan. 2017. "Observations of an Extra-Large Subsurface Anticyclonic Eddy in the Northwestern Pacific Subtropical Gyre." *Journal of Marine Science: Research & Development* 7, no. 4: 1000235. https://doi.org/10.4172/2155-9910.1000235.

Nelson, C. E., C. A. Carlson, C. S. Ewart, and E. R. Halewood. 2014. "Community Differentiation and Population Enrichment of Sargasso Sea Bacterioplankton in the Euphotic Zone of a Mesoscale Mode-Water Eddy." *Environmental Microbiology* 16, no. 3: 871–887. https://doi.org/10.1111/1462-2920.12241.

Parsons, T. R., Y. Maita, and C. M. Lalli. 1984. A Manual of Chemical and Biological Methods for Seawater Analysis. Pergamon Press.

Pelusi, A., P. De Luca, F. Manfellotto, K. Thamatrakoln, K. D. Bidle, and M. Montresor. 2021. "Virus-Induced Spore Formation as a Defense Mechanism in Marine Diatoms." *New Phytologist* 229: 2251–2259. https://doi.org/10.1111/nph.16951.

Pierce, R. W., and J. T. Turner. 1992. "Ecology of Planktonic Ciliates in Marine Food Webs." *Reviews in Aquatic Sciences* 6, no. 2: 139–181.

Qi, Y., H. Mao, Y. Du, et al. 2022. "A Lens-Shaped, Cold-Core Anticyclonic Surface Eddy in the Northern South China Sea." *Frontiers in Marine Science* 9: 976273. https://doi.org/10.3389/fmars.2022.976273.

Quast, C., E. Pruesse, P. Yilmaz, et al. 2013. "The SILVA Ribosomal RNA Gene Database Project: Improved Data Processing and Web-Based Tools." *Nucleic Acids Research* 41: D590–D596. https://doi.org/10.1093/nar/gks1219.

Roggenbuck, M., I. Bærholm Schnell, N. Blom, et al. 2014. "The Microbiome of New World Vultures." *Nature Communications* 5: 5498. https://doi.org/10.1038/ncomms6498.

Romero, O. E., G. Fischer, J. Karstensen, and P. Cermeño. 2016. "Eddies as Trigger for Diatom Productivity in the Open-Ocean Northeast Atlantic." *Progress in Oceanography* 147: 38–48. https://doi.org/10.1016/j.pocean.2016.07.011.

Ruvindy, R., A. Barua, C. J. S. Bolch, C. Sarowar, H. Savela, and S. A. Murray. 2023. "Genomic Copy Number Variability at the Genus, Species and Population Levels Impacts In Situ Ecological Analyses of Dinoflagellates and Harmful Algal Blooms." *ISME Communications* 3: 70. https://doi.org/10.1038/s43705-023-00274-0.

Sasai, Y., A. Ishida, H. Sasaki, S. Kawahara, H. Uehara, and Y. Yamanaka. 2006. "A Global Eddy-Resolving Coupled Physical-Biological Model: Physical Influences on a Marine Ecosystem in the North Pacific." *Simulation* 82: 467–474. https://doi.org/10.1177/0037549706068943.

Sheyn, U., K. E. Poff, J. M. Eppley, et al. 2025. "Mesoscale Eddies Shape *Prochlorococcus* Community Structure and Dynamics in the Oligotrophic Open Ocean." *The ISME Journal* 19, no. 1: wraf106. https://doi.org/10.1093/ismejo/wraf106.

Simmons, S., A. Sudek, A. Monier, et al. 2016. "Abundance and Biogeography of Picoprasinophyte Ecotypes and Other Phytoplankton in the Eastern North Pacific Ocean." *Applied and Environmental Microbiology* 82, no. 6: 1693–1705. https://doi.org/10.1128/AEM.02730-15.

Spingys, C. P., R. G. Williams, R. E. Tuerena, et al. 2021. "Observations of Nutrient Supply by Mesoscale Eddy Stirring and Small-Scale Turbulence in the Oligotrophic North Atlantic." *Global Biogeochemical Cycles* 35, no. 12: e2021GB007200. https://doi.org/10.1029/2021GB007200.

Stoeck, T., D. Bass, M. Nebel, et al. 2010. "Multiple Marker Parallel Tag Environmental DNA Sequencing Reveals a Highly Complex Eukaryotic Community in Marine Anoxic Water." *Molecular Ecology* 19: 21–31. https://doi.org/10.1111/j.1365-294X.2009.04480.x.

Stoecker, D. K., P. J. Hansen, D. A. Caron, and A. Mitra. 2017. "Mixotrophy in the Marine Plankton." *Annual Review of Marine Science* 9, no. 1: 311–335. https://doi.org/10.1146/annurev-marine-010816-060617.

Sun, P., Y. Wang, X. Huang, et al. 2024. "Cracking the Dynamic Code of the Deep: Unexpected Seasonal Patterns of Active Protistan-Bacterial Microbiomes in the Mesopelagic Zone of the South China Sea." *Progress in Oceanography* 225: 103280. https://doi.org/10.1016/j.pocean.2024.103280.

Sun, W., Y. Liu, G. Chen, W. Tan, X. Lin, and Y. Guan. 2021. "Three-Dimensional Properties of Mesoscale Cyclonic Warm-Core and Anticyclonic Cold-Core Eddies in the South China Sea." *Acta Oceanologica Sinica* 40, no. 10: 17–29. https://doi.org/10.1007/s13131-021-1770-x.

Takikawa, T., H. Ichikawa, K. Ichikawa, and S. Kawae. 2005. "Extraordinary Subsurface Mesoscale Eddy Detected in the Southeast of Okinawa in February 2002." *Geophysical Research Letters* 32, no. 17: L17602. https://doi.org/10.1029/2005GL023842.

Waga, H., T. Hirawake, and H. Ueno. 2019. "Impacts of Mesoscale Eddies on Phytoplankton Size Structure." *Geophysical Research Letters* 46, no. 22: 13191–13198. https://doi.org/10.1029/2019GL085150.

Wang, L., B. Huang, E. A. Laws, et al. 2018. "Anticyclonic Eddy Edge Effects on Phytoplankton Communities and Particle Export in the Northern South China Sea." *Journal of Geophysical Research: Oceans* 123: 7632–7650. https://doi.org/10.1029/2017JC013623.

Wang, Y., J. Yang, and G. Chen. 2023. "Euphotic Zone Depth Anomaly in Global Mesoscale Eddies by Multi-Mission Fusion Data." *Remote Sensing* 15: 1062. https://doi.org/10.3390/rs15041062.

Wu, J., Z. Lee, Y. Xie, et al. 2021. "Reconciling Between Optical and Biological Determinants of the Euphotic Zone Depth." *Journal of Geophysical Research. Oceans* 126: e2020JC016874. https://doi.org/10.1029/2020JC016874.

Xu, W., G. Wang, X. Cheng, et al. 2023. "Mesoscale Eddy Modulation of Subsurface Chlorophyll Maximum Layers in the South China Sea." *Journal of Geophysical Research. Biogeosciences* 128, no. 11: e2023JG007648. https://doi.org/10.1029/2023JG007648.

Yang, G. B., Q. Zheng, X. J. Xiong, et al. 2019. "Subsurface Cyclonic Eddies Observed in the Southeastern Tropical Indian Ocean." *Journal of Geophysical Research: Oceans* 124, no. 10: 7247–7260. https://doi.org/10.1029/2019JC015381.

Zhou, K., M. Dai, S.-J. Kao, et al. 2013. "Apparent Enhancement of ^{234}Th-Based Particle Export Associated With Anticyclonic Eddies." *Earth and Planetary Science Letters* 381: 198–209. https://doi.org/10.1016/j.epsl.2013.07.039.

Zinger, L., A. Gobet, and T. Pommier. 2012. "Two Decades of Describing the Unseen Majority of Aquatic Microbial Diversity." *Molecular Ecology* 21, no. 8: 1878–1896. https://doi.org/10.1111/j.1365-294X.2011.05362.x.

Supporting Information

Additional Supporting Information may be found in the online version of this article.

Submitted 03 August 2025
Revised 09 December 2025
Accepted 15 March 2026